Structure, magnetization, specific heat, and microwave properties of $K_x Fe_{2-y}Se_2$

2016 Supercond. Sci. Technol. 29 085015

(http://iopscience.iop.org/0953-2048/29/8/085015)

IOP Publishing Superconductor Science and Technology
Supercond. Sci. Technol. 29 (2016) 085015 (6pp) doi:10.1088/0953-2048/29/8/085015

Structure, magnetization, specific heat, and microwave properties of $K_xFe_{2-y}Se_2$

D Yazici[1,2,5,6], Ali C Basaran[1,2,3], J G Ramírez[1,2,4], Ivan K Schuller[1,2,6] and M B Maple[1,2,6]

[1] Department of Physics, University of California, San Diego, La Jolla, CA 92093, USA
[2] Center for Advanced Nanoscience, University of California, San Diego, La Jolla, CA 92093, USA
[3] Department of Physics, Gebze Technical University, Gebze, Kocaeli 41400, Turkey
[4] Department of Physics, Universidad de los Andes, Bogotá 111711, Colombia

E-mail: duygu@physics.ucsd.edu, ischuller@ucsd.edu and mbmaple@ucsd.edu

Received 8 April 2016, revised 7 June 2016
Accepted for publication 24 June 2016
Published 11 July 2016

Abstract

Temperature-dependent magnetization, specific heat, and magnetic field modulated microwave spectroscopy (MFMMS) measurements were performed on single crystals of $K_xFe_{2-y}Se_2$. Magnetization measurements yield a superconducting transition temperature (T_c) of ~30 K, with a diamagnetic shielding fraction of nearly 90%. Specific heat measurements revealed a 'jump' at T_c, $\Delta C/T|_{T_c}$, of about 6.8 ± 1 mJ mol^{-1} K^{-2}, consistent with bulk superconductivity in $K_xFe_{2-y}Se_2$. Moreover, MFMMS measurements detect the superconductivity of $K_xFe_{2-y}Se_2$ with a peak with an onset at $T_c^{\mu} \sim 28$ K, close to the values of T_c determined from the magnetization and specific heat measurements. The presence and the shape of the low temperature MFMMS signal could be ascribed to a complex dissipation mechanism and percolative superconductivity.

Keywords: superconductivity, microwave properties, specific heat

(Some figures may appear in colour only in the online journal)

1. Introduction

The discovery of superconductivity in Fe-pnictides and chalcogenides has generated great interest in these materials because of their high superconducting transition temperatures (T_c) and the proximity of the superconductivity to long-range magnetic order in the form of antiferromagnetism or spin density waves [1–6]. In particular, FeSe and its intercalated variants $A_xFe_{2-y}Se_2$ (A = alkali metal) have been extensively investigated [7–16]. Even though the crystal structure of these compounds is identical to that of 122-type Fe-pnictides ($BaFe_2As_2$, $CaFe_2As_2$) [17, 18], they exhibit more complex magnetic and structural features. For instance, $A_xFe_{2-y}Se_2$ compounds exhibit static long-range antiferromagnetic (AFM) order with a high Néel temperature $T_N \approx 560$ K [19]. The Fe saturation moment in the AFM phase is $3.3\mu_B$, which is the largest magnetic moment observed in all Fe-based superconductors. Due to the proximity of superconductivity and AFM order in these Fe-based compounds, the magnetism becomes a central issue. Still an open question is whether the coexistence of superconductivity and AFM ordering is at the microscopic level or if these are two different spatially interspersed phases. $K_xFe_{2-y}Se_2$ compounds have a width of formation, show a strong dependence of electrical transport properties on their stoichiometry/Fe vacancy concentration, and are in very close proximity to an insulating state [7, 14, 20]. Due to the off-stoichiometric nature of $K_xFe_{2-y}Se_2$, wide ranges of the values of x and y ($0.6 \leqslant x \leqslant 1$; $0 \leqslant y \leqslant 0.59$) have been reported for the superconducting crystals with similar T_c values (~31–33 K) by several groups [7, 8, 12, 13, 15, 16, 20–23]. The broad feature in its normal state electrical resistivity data, which is ascribed to the ordering of Fe vacancies [7, 12, 13, 22] and the percolative superconductivity investigated via magnetization measurements [24], suggest that the superconductivity

[5] Current address: Faculty of Health Sciences, Artvin Coruh University, 08000 Artvin, Turkey.
[6] Authors to whom any correspondence should be addressed.

and its relationship with structural and magnetic order need to be investigated further.

In this manuscript, we provide the growth details, magnetization and specific heat measurements, as well as magnetic field modulated microwave spectroscopy (MFMMS) measurements [25] on $K_xFe_{2-y}Se_2$ single crystals.

2. Experimental details

Single crystals of $K_xFe_{2-y}Se_2$ were prepared by melting an FeSe precursor and K metal. The FeSe precursor was prepared by reacting stoichiometric amounts of Fe and Se at 1050 °C. Then, K and FeSe with a nominal composition of KFe_2Se_2 were sealed in an evacuated quartz tube. Due to the reaction of the potassium with the quartz tube, this primary ampoule was sealed within a secondary, larger quartz tube to prevent exposure to air if the first ampoule degraded enough to crack. The KFe_2Se_2 charge was placed in a furnace heated to 1080 °C where it was held for 4 h. The furnace temperature was then slowly lowered to 780 °C over 50 h, and allowed to cool naturally for an additional 10 h to room temperature. Once the ampoules were opened, large (up to $5 \times 2 \times 0.5$ mm^3), dark, shiny crystals were mechanically separated from the solidified melt. The crystals are very air-sensitive and were handled under an Ar atmosphere. Since the actual composition of the resultant single crystals was not determined and their off-stoichiometric nature is well known, we use $K_xFe_{2-y}Se_2$ to denote the single crystals whose measurements are reported in this manuscript.

The orientation of single crystals, crystal structure and sample quality were primarily characterized through analysis of XRD powder patterns collected with a Bruker D8 Discover x-ray diffractometer. Magnetization measurements were performed between 5 to 300 K in a Quantum Design Magnetic Property Measurement System (MPMS), equipped with a 7 T superconducting magnet. Specific heat measurements were performed down to 1.8 K using a Quantum Design Physical Property Measurement System, DynaCool. The heat capacity measurements were made using a standard thermal relaxation technique. Magnetic field modulated microwave spectroscopy (MFMMS) measurements were performed using a customized Bruker EleXsys X-band (9.4 GHz) electron paramagnetic resonance apparatus. The spectrometer was operated in a non-conventional mode where the microwave absorption signal was measured as a function of temperature [25]. A small (15 Oe) external magnetic field was applied and maintained during the measurement. A 100 kHz modulation field was used with a peak-to-peak amplitude of 15 Oe. As a result, the total applied magnetic field was always positive to avoid field-dependent hysteretic effects. A flake of a single crystal sample was placed in a high purity quartz tube which was filled with helium gas and sealed. The sample was placed in the center of a rectangular dual mode cavity with microwave magnetic field parallel to the modulation and external magnetic fields. The applied microwave power was chosen to be low enough (1 mW) to avoid heating. A flow cryostat was used to sweep the temperature from 300 to 4 K with a rate of 5 K min^{-1}.

3. Results and discussion

Powder x-ray diffraction patterns were measured over a range of 2θ values ($10 \leqslant 2\theta \leqslant 70$) for $K_xFe_{2-y}Se_2$ (single crystals were crushed and powdered using a mortar and pestle). The broad background in the XRD pattern is associated with the glass substrate. Analysis of the powder x-ray diffraction pattern indicate that the $K_xFe_{2-y}Se_2$ single crystals consist of a single phase without any trace of impurity phases. Rietveld refinements were performed on the XRD powder pattern for the $K_xFe_{2-y}Se_2$ single crystals using GSAS [26] and EXPGUI [27]. The lattice parameters obtained using this procedure, $a = b = 3.88$ Å and $c = 14.25$ Å, are in agreement with previous reports [7, 21]. The $ThCr_2Si_2$-type tetragonal crystal structure with *I4/mmm* space group was observed for $K_xFe_{2-y}Se_2$. An XRD pattern for the $K_xFe_{2-y}Se_2$ single crystals is shown in figure 1 and plotted with the refined pattern for comparison (weighted residual value $wR_p = 0.0474$).

Shown in figure 2 are zero-field cooled (ZFC) and field-cooled (FC) direct current (dc) magnetization M versus temperature T data for $K_xFe_{2-y}Se_2$ single crystals measured in an applied magnetic field $H = 5$ Oe with the magnetic field applied parallel to the *ab* plane. The sharp superconducting transition around $T_c \sim 30$ K reflects the good quality of the single crystal. The superconductive shielding fraction estimated from the ZFC magnetization at 10 K is about 90%, demonstrating that the $K_xFe_{2-y}Se_2$ single crystals exhibit bulk superconductivity. Similar superconductive shielding fractions have been reported by Ying *et al* [7]. However, this superconductive shielding fraction is much larger than that reported in several other previous reports [11, 14, 21]. In the temperature range from room temperature to T_c (not shown here), the ZFC and FC magnetization curves are essentially flat and temperature independent, indicating that the sample is a Pauli paramagnet.

Isothermal magnetization M versus H curves were measured at various temperatures with the magnetic field applied parallel to the *ab* plane. Selected M versus H isotherms measured at $T = 5$, 10, 15, 20, and 35 K are shown in figure 3. The M versus H plot at $T = 35$ K, which is above T_c, shows slightly hysteretic behavior at low magnetic fields. This might be related to the inclusion of Fe as an impurity phase. By extrapolating the high-field slope of the magnetization curve at 35 K back to $H = 0$ T, the saturation moment μ_{sat} was determined to be ~0.01 μ_B f.u.$^{-1}$ which suggests that the crystal has ~0.5 of pure % Fe inclusions. However, the XRD pattern did not indicate the presence of any impurity phases in the crystals within the resolution of the XRD measurements (several percent). In the Meissner state, the M versus H curves are linear. The lower critical field $H_{c1}(T)$, defined as the field in which M versus H deviates from linearity, is ~120 Oe at $T = 5$ K and decreases with increasing T.

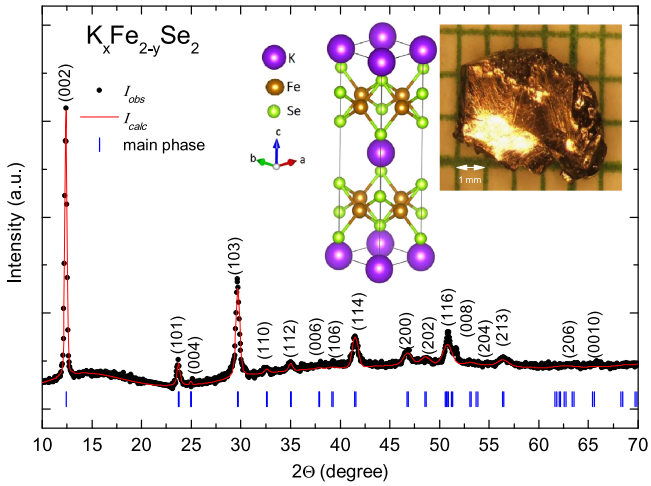

Figure 1. X-ray diffraction pattern for $K_xFe_{2-y}Se_2$ measured at room temperature. The black circles indicate the observed intensity I_{obs} for $K_xFe_{2-y}Se_2$. All the peaks can be well indexed. The red line represents the calculated intensity I_{calc}. Tick marks represent calculated peak positions of the main phase. The left-inset shows the schematic crystal structure of $K_xFe_{2-y}Se_2$ ($ThCr_2Si_2$ type). A picture of a $K_xFe_{2-y}Se_2$ single crystal is shown in the right-inset where the small squares are 1 mm × 1 mm for reference.

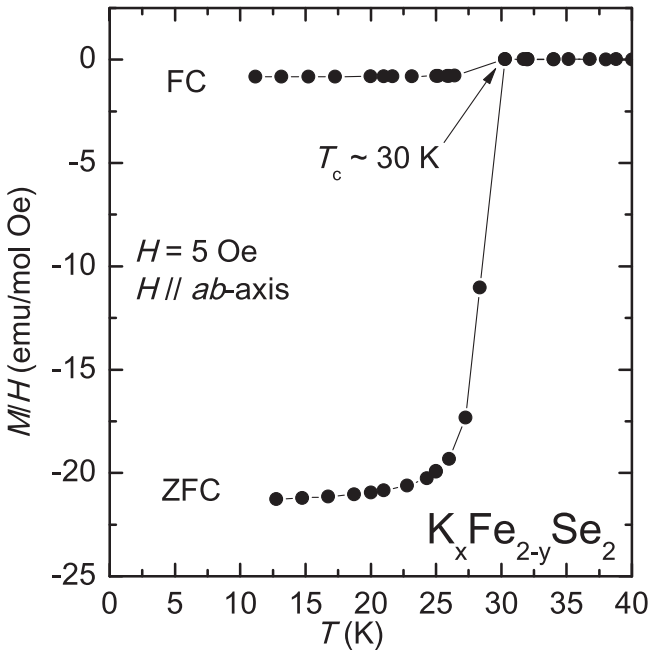

Figure 2. (a) Zero-field cooled (ZFC) and field-cooled (FC) dc magnetic susceptibility M/H versus temperature T data for $K_xFe_{2-y}Se_2$ measured in an applied magnetic field of $H = 5$ Oe with the magnetic field applied parallel to the ab plane. The superconducting transition temperature, T_c, is indicated by an arrow.

M versus H data at selected temperatures with H applied parallel to the ab-plane for $K_xFe_{2-y}Se_2$ are plotted in figure 3. Left inset of the figure indicates the temperature dependence of upper critical field H_{c2}(kOe) for $K_xFe_{2-y}Se_2$. The red dashed line indicates the linear extrapolation of temperature to 0 K which approach a value of 11.6 kOe. According to the conventional one-band Werthamer–Helfand–Hohenberg

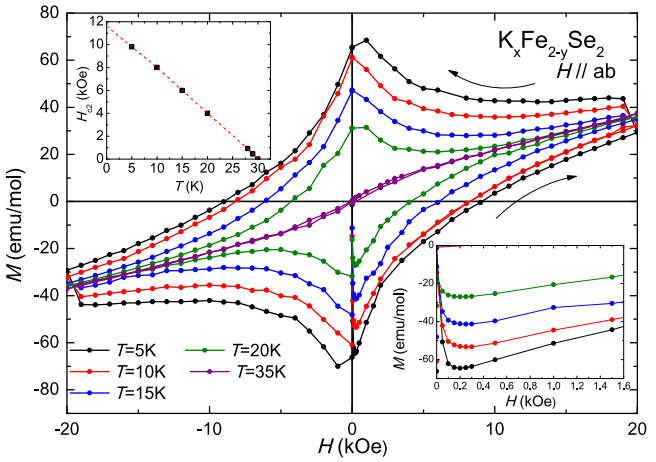

Figure 3. M versus H data at selected temperatures with H applied parallel to the ab-plane for $K_xFe_{2-y}Se_2$. Left inset: the temperature dependence of upper critical field H_{c2}(kOe) for $K_xFe_{2-y}Se_2$. The red dashed line indicates the linear extrapolation of temperature to 0 K. Right inset: low-magnetic field M versus H curves at various temperatures.

(WHH) theory [28], $H_{c2}(0) = -0.69T_c(dH_{c2}/dT)_{T_c}$. H_{c2} values for various temperatures were derived from the M versus H isotherms in figure 3 as the field where the irreversibility disappears. The zero temperature value of the orbital critical field $H_{c2}(0)\|ab$-plane for the $K_xFe_{2-y}Se_2$ compound was inferred from the initial slopes of the H_{c2} versus T curve, $-(dH_{c2}/dT)_{T_c} = 0.57$ kOe K^{-1}, yielding a value of ~12 kOe, which is smaller than that estimated for the same orientation in $K_{0.8}Fe_{1.8}Se_2$ [29]. It is well accepted that the WHH formula is valid for one-band superconductors and that $H_{c2}(0)$ might be affected by the complicated multiband structure as observed in various FeSe compounds [3, 4]. Hence, the value of $H_{c2}(0)$ derived from the initial slope of the $H_{c2}(T)$ curve is just a rough estimate. An accurate value of $H_{c2}(0)$ can only be achieved by applying high enough magnetic fields.

Plots of specific heat divided by temperature C/T versus T for $K_xFe_{2-y}Se_2$ in zero magnetic field, $C(T, H = 0)/T$, and in a magnetic field of 9 T, $C(T, H = 9\,\mathrm{T})/T$, with the magnetic field applied parallel to the c-axis, are presented in figure 4(a). At around 30 K, there is a small peak in the $C(T)/T$ data of $K_xFe_{2-y}Se_2$ that coincides with the feature in $M(T)/H$, indicative of a phase transition. The $C(T)/T$ data were analyzed by performing linear fits of the expression $C(T)/T = \gamma + \beta T^2$ to the data plotted as C/T versus T^2 shown in figure 4(b), where γ and β are the electronic and phonon contributions to the specific heat, respectively. Since the $K_xFe_{2-y}Se_2$ sample is superconducting below 30 K, the electronic specific heat coefficient γ is expected to depend on temperature, exhibiting a 'jump' in magnitude at T_c and then decreasing with T exponentially for a nodeless superconducting energy gap or as a power law for a nodal gap. However, since γ is small, we treat it as a constant in the analysis of the $C(T)/T$ data as we would if the sample were to be in the normal state over the entire temperature range of the fit. As a conservative rule of thumb, performing a linear fit

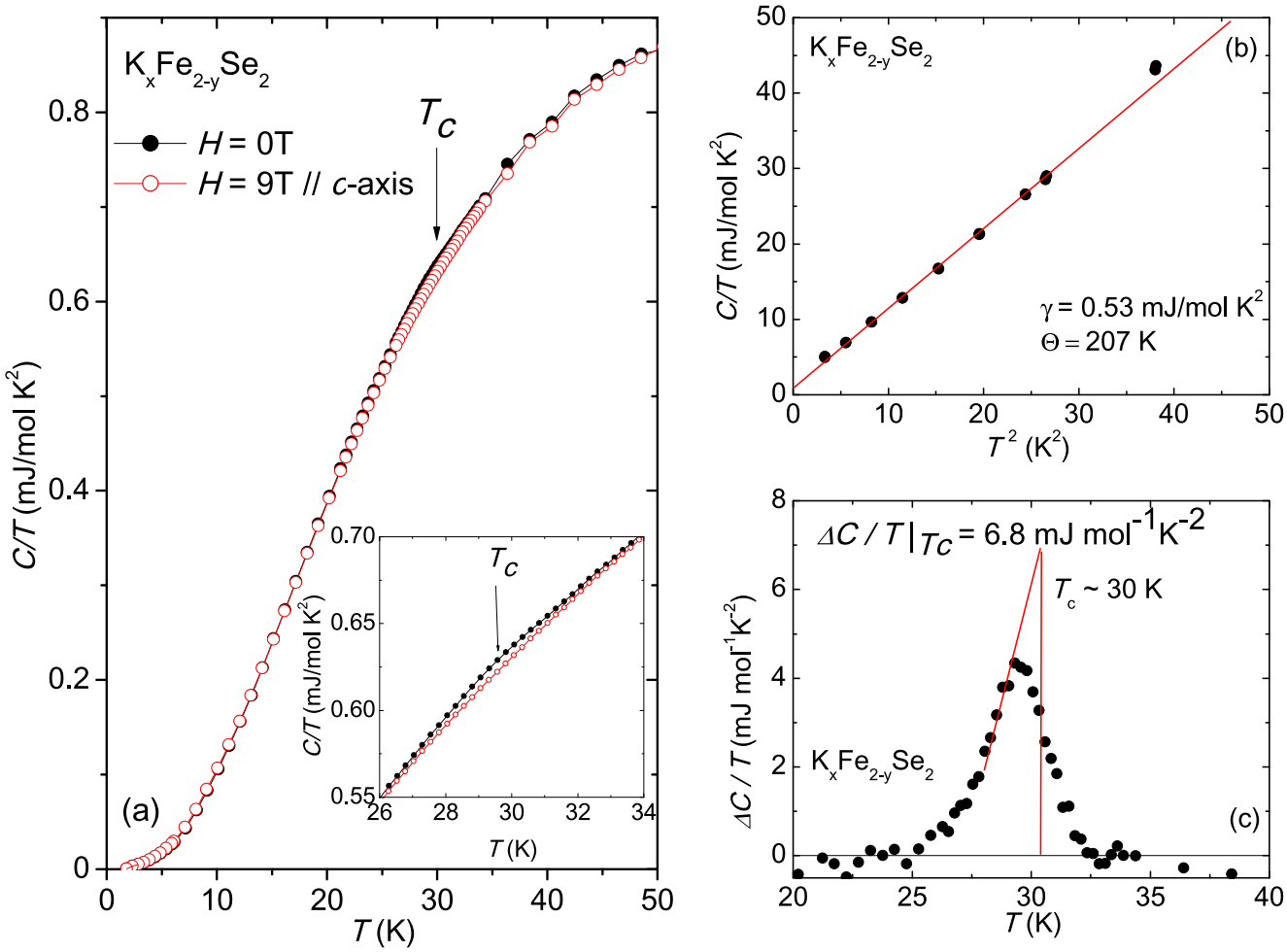

Figure 4. (a) Specific heat divided by temperature C/T for $K_xFe_{2-y}Se_2$ in zero magnetic field (solid black circles) and in an applied magnetic field $H = 9$ T with the magnetic field applied parallel to the c-axis (open red circles). Inset: specific heat divided by temperature C/T at temperatures close to the superconducting transition temperature T_c emphasizing the T_c (indicated by an arrow).(b) C/T versus T^2 for $K_xFe_{2-y}Se_2$. The solid red line represents a fit to the data using the equation $C(T)/T = \gamma + \beta T^2$. (c) The difference in the $C(T)/T$ data between zero magnetic field and in an applied magnetic field of $H = 9$ T. A value for the superconducting transition temperature T_c of ~30.5 K was extracted from an equal area entropy conserving construction. The red solid line is a guide to the eye to show how the height of the specific heat anomaly was estimated.

of the $C(T)/T$ versus T^2 data to extract γ and calculate Θ_D from β is reasonable up to a maximum temperature of $\sim\Theta_D/50$ [30]. Guided by this rule, the fits were performed in the 4–30 K^2 temperature range and yielded the values $\gamma \approx 0.53$ mJ mol^{-1} K^{-2} and $\beta \approx 1.1$ mJ mol^{-1} K^{-4}. Using the relation: $\Theta_D = \left(\frac{12\pi^4}{5\beta} nR\right)^{1/3}$, where $R = 8.3145$ J mol^{-1} K^{-1} is the ideal gas constant and $n = 5$ is the number of atoms in one unit cell [31], the Debye temperature was calculated and found to be $\Theta_D \approx 207$ K, which is relatively small compared to other FeAs-based superconductors [3]. The small residual electronic coefficient γ at low temperatures in the superconducting state could be evidence for a nodal gap in $K_xFe_{2-y}Se_2$ which is consistent with NMR measurements [3].

The specific heat anomaly due to the superconductivity in the vicinity of T_c at zero field is more visible in figure 4(c), which shows the difference between the $C(T)/T$ data for $H = 0$ T and $H = 9$ T. Assuming this feature is indeed due to the transition into the superconducting state, we can estimate $T_c \sim 30.5$ K from an equal area entropy conserving construction (red lines in figure 4(c)). This value of T_c is close to the the value ($T_c \sim 30$ K) obtained from the magnetization. The presence of the feature suggests that superconductivity in $K_xFe_{2-y}Se_2$ is a bulk phenomenon. We can estimate the value of the specific heat jump $\Delta C/T|_{T_c}$ at T_c from the height of the entropy conserving construction which yields about 6.8 ± 1 mJ mol^{-1} K^{-2}. If we use the value of the normal state electronic specific heat coefficient $\gamma_n = 5.8$ mJ mol^{-1} K^{-2} reported by Zeng *et al* [32], $\Delta C/\gamma_n T \approx 1.2$ for $K_xFe_{2-y}Se_2$, which is close to the weak coupling BCS value. However, due to the difficulty of estimating the normal state electronic contribution γ_n, a reliable conclusion about the coupling strength can not be made.

In addition to the aforementioned standard superconducting analysis of the $K_xFe_{2-y}Se_2$ single crystals, we used magnetic MFMMS [25, 33] to investigate the superconductivity and its relationship with other types of electronic

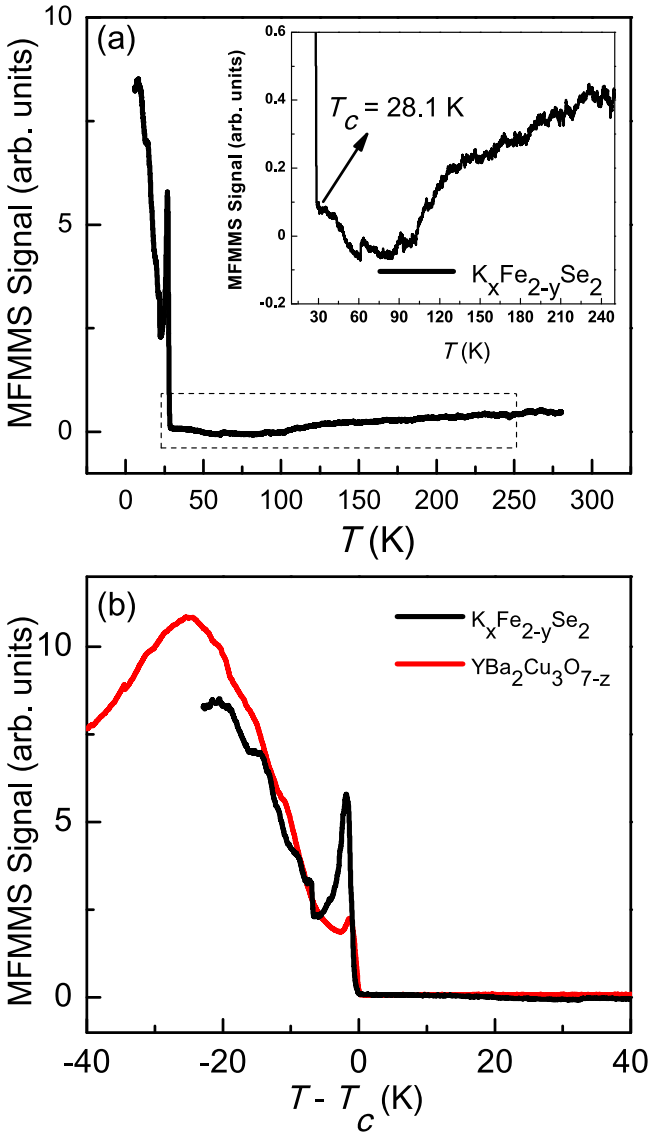

Figure 5. (a) Magnetic field modulated microwave spectroscopy (MFMMS) of $K_xFe_{2-y}Se_2$. A small (15 Oe) external magnetic field was applied and maintained during the measurement. The MFMMS signal was recorded in a rectangular X-band cavity at 9.4 GHz microwave frequency. A 100 kHz modulation field was used with a peak-to-peak amplitude of 15 Oe. The superconducting transition appears as a sharp peak with an onset $\sim T_c^{\mu} \sim 28$ K. The inset is zoomed into the dotted area above the superconducting transition. (b) MFMMS signal of $K_xFe_{2-y}Se_2$ (black) compared to that of high-T_c superconducting $YBa_2Cu_3O_{7-z}$ powder (red). In order to qualitatively compare the MFMMS signal of these two materials, the signal is plotted versus T–T_c for each sample.

and magnetic order in these compounds. MFMMS is mainly used to screen for the presence of possible superconducting transitions in a given temperature range. However, there are other electromagnetic transitions and microwave absorption mechanisms that can be detected by this technique [25, 34]. Therefore, the complex phase diagram of alkali metal doped FeSe compounds and its strong relation with other mechanisms could be further investigated. Inclusion of Fe at the level of ~0.5%, estimated from M versus H measurements performed at $T = 35$ K, and other possible impurity phases can be detected by MFMMS, which makes it possible to probe all phases present in the sample at the same time with very high sensitivity [25, 33].

Figure 5(a) shows the MFMMS signal of a single crystal of $K_xFe_{2-y}Se_2$ over a broad temperature range. The superconducting transition appears as a sharp peak with an onset at ~28 K, which is close to the temperature obtained from the magnetization and specific heat measurements. At the transition of a superconducting material, the main characteristic of the MFMMS signal for low dc fields is generally manifested as follows: the signal is in the noise floor for temperatures above T_c^{μ} and increases abruptly at the T_c^{μ}. The signal reaches a maximum at a certain temperature and decreases back to the noise level measured above T_c^{μ} [25]. This typical MFMMS response is observed for various superconductors such as MgB_2, $ErRh_4B_4$, and Nb [25]. However, this is not the case for $K_xFe_{2-y}Se_2$: the absorption signal increases with decreasing temperature after the transition. Similar non-zero low temperature microwave absorption signals have been observed in many high-T_c cuprates [35, 36]. We measured the MFMMS signal of superconducting $YBa_2Cu_3O_{7-z}$ powder and qualitatively compared it to the MFMMS signal of $K_xFe_{2-y}Se_2$ in figure 5(b). The absorption signal below T_c^{μ} for both samples shows surprisingly similar trends. The non-zero absorption signal indicates that there are additional dissipation mechanisms which give rise to the low temperature MFMMS signal in the superconducting phase. This dissipation mechanism might be vortex motion and pinning, a Bragg glass-vortex liquid transition, or Josephson junctions (weak links) which can be detected by MFMMS [25].

The low temperature microwave absorption signal in cuprates is generally attributed to an ensemble of weak links or Josephson junctions between superconducting regions in the bulk samples [37]. It is generally accepted that high-T_c superconductors consist of weakly coupled grains—even in single crystals [38]. The grain size and coupling strength depend on the preparation process and the sample morphology. It is this granularity which is probed very efficiently by the microwave absorption technique. Therefore, the low temperature MFMMS signal could be ascribed to the presence of weak links in $K_xFe_{2-y}Se_2$. This is in agreement with the previously observed intrinsic percolative superconductivity in $K_xFe_{2-y}Se_2$ compounds at low temperatures [24].

In the high temperature region (the inset of figure 5(a)), the slight change at ~120 K in the absorption signal is similar to the ones observed in magnetite due to the Verwey transition [34]. Considering the magnetization measurements that indicate the presence of a small magnetic background (~0.5% Fe inclusion) above the superconducting transition and the extreme sensitivity of the MFMMS technique, it is likely that the surface of the sample is slightly oxidized.

4. Summary

In summary, we prepared a K-intercalated FeSe compound, $K_xFe_{2-y}Se_2$, in single crystalline form, with a value of T_c of

~30 K. The ZFC dc magnetization measurements indicate that the superconductive shielding fraction is close to 90%, which shows that the crystals exhibit bulk superconductivity and are of good quality. A specific heat anomaly is observed at $T_c \approx 30.5$ K with a specific heat 'jump' $\Delta C/T|_{T_c}$ of $\sim 6.8 \pm 1\,\mathrm{mJ\,mol^{-1}\,K^{-2}}$. The ratio $\Delta C/\gamma_n T \approx 1.2$ for $K_xFe_{2-y}Se_2$ is close to the weak coupling BCS value. MFMMS measurements confirm the superconductivity of $K_xFe_{2-y}Se_2$ sample with an onset at $T_c^{\mu} \sim 28$ K, close to the T_c determined from the magnetization and specific heat measurements. The presence and the shape of the low temperature MFMMS signal could be ascribed to a complex dissipation mechanism and percolative superconductivity similar to what is found in the high-T_c cuprate superconductors.This dissipation mechanism is generally caused by weak links which can be detected by MFMMS. The small drop in the MFMMS signal at ~120 K is similar to the Verwey transition of magnetite and could be due to slight oxidation on the surface.

Acknowledgments

This research was supported by the US Department of Energy, Office of Basic Energy Sciences, Division of Materials Sciences and Engineering under Grant No. DE-FG02-04ER46105 (sample synthesis, characterization, and physical properties measurements) and by the AFOSR under Grant No. FA9550-14-1-0202 (structural characterization and MFMMS measurements). Conception of the experiments and writing of the manuscript were done by multiple interactions between all of the authors.

References

[1] Hosono H 2008 *J. Phys. Soc. Japan* **77** 1
[2] Ishida K and Hosono H Y N 2009 *J. Phys. Soc. Japan* **78** 062001
[3] Paglione J and Greene R L 2010 *Nat. Phys.* **6** 645
[4] Mazin I I 2010 *Nature* **464** 183
[5] Lumsden M D and Christianson A D 2010 *J. Phys.: Condens. Matter* **22** 203203
[6] Li W *et al* 2012 *Phys. Rev. Lett.* **109** 057003
[7] Ying J J *et al* 2011 *Phys. Rev.* B **83** 212502
[8] Li C H, Shen B, Han F, Zhu X and Wen H H 2011 *Phys. Rev.* B **83** 184521
[9] Fang M H, Wang H D, Dong C H, Li Z J, Feng C M, Chen J and Yuan H Q 2011 *Europhys. Lett.* **94** 27009
[10] Medvedev S *et al* 2009 *Nat. Mater.* **8** 630
[11] Mizuguchi Y, Takeya H, Kawasaki Y, Ozaki T, Tsuda S, Yamaguchi T and Takano Y 2011 *Appl. Phys. Lett.* **98** 042511
[12] Qian T *et al* 2011 *Phys. Rev. Lett.* **106** 187001
[13] Shein I and Ivanovskii A 2011 *Phys. Lett.* A **375** 1028
[14] Wang D M, He J B, Xia T L and Chen G F 2011 *Phys. Rev.* B **83** 132502
[15] Zhang Y *et al* 2011 *Nat. Mater.* **10** 273
[16] Zavalij P *et al* 2011 *Phys. Rev.* B **83** 132509
[17] Sasmal K, Lv B, Lorenz B, Guloy A M, Chen F, Xue Y Y and Chu C W 2008 *Phys. Rev. Lett.* **101** 107007
[18] Rotter M, Tegel M and Johrendt D 2008 *Phys. Rev. Lett.* **101** 107006
[19] Wei B, Qing-Zhen H, Gen-Fu C, Green M A, Du-Ming W, Jun-Bao H and Yi-Ming Q 2011 *Chin. Phys. Lett.* **28** 086104
[20] Wang X C, Liu Q Q, Lv Y X, Gao W B, Yang L X, Yu R C, Li F Y and Jin C Q 2008 *Solid State Commun.* **148** 538
[21] Guo J, Jin S, Wang G, Wang S, Zhu K, Zhou T, He M and Chen X 2010 *Phys. Rev.* B **82** 180520
[22] Mizuguchi Y, Hara Y, Deguchi K, Tsuda S, Yamaguchi T, Takeda K, Kotegawa H, Touand H and Takano Y 2010 *Supercond. Sci. Technol.* **23** 054013
[23] Torchetti D A, Fu M, Christensen D C, Nelson K J, Imai T, Lei H C and Petrovic C 2011 *Phys. Rev.* B **83** 104508
[24] Shen B, Zeng B, Chen G F, He J B, Wang D M, Yang H and Wen H H 2011 *Europhys. Lett.* **96** 37010
[25] Ramírez J G, Basaran A C, de la Venta J, Pereiro J and Schuller I K 2014 *Rep. Prog. Phys.* **77** 093902
[26] Larson A C and Von Dreele R B 2000 General structure analysis system (GSAS), *Technical Report* LAUR (Los Alamos, NM: Los Alamos National Laboratory)
[27] Toby B H 2001 *J. Appl. Crystallogr.* **34** 210
[28] Werthamer N R, Helfand E and Hohenberg P C 1966 *Phys. Rev.* **147** 295
[29] Mun E D, Altarawneh M M, Mielke C H, Zapf V S, Hu R, Bud'ko S L and Canfield P C 2011 *Phys. Rev.* B **83** 100514
[30] Gopal E S R 1966 *Specific Heat at Low Temperatures* (New York: Plemum)
[31] Kittel C 1996 *Introduction to Solid State Physics* 7th edn (Canada: Wiley)
[32] Zeng B, Shen B, Chen G F, He J B, Wang D M, Li C H and Wen H H 2011 *Phys. Rev.* B **83** 144511
[33] Kim B F, Bohandy J, Moorjani K and Adrian F J 1988 *J. Appl. Phys.* **63** 2029
[34] Guenon S, Ramirez J G, Basaran A C, Wampler J, Thiemens M, Taylor S and Schuller I K 2014 *Sci. Rep.* **4** 7333
[35] Bohandy J, Adrian F J, Kim B F, Moorjani K, Shull R D, Swartzendruber L J, Bennett L H and Wallace J S 1988 *J. Supercond.* **1** 191
[36] Moorjani K, Bohandy J, Adrian F J, Kim B F, Shull R D, Chiang C K, Swartzendruber L J and Bennett L H 1987 *Phys. Rev.* B **36** 4036
[37] Dulcic A, Rakvin B and Pozek M 1989 *Europhys. Lett.* **10** 593
[38] Deutscher G and Müller K A 1987 *Phys. Rev. Lett.* **59** 1745